Effects of sputtering conditions on low-pressure radio-frequency discharge

D. Wan and K. Komvopoulos

Department of Mechanical Engineering, University of California, Berkeley, CA 94720

Abstract

The characteristics of low-pressure (< 10 mTorr) Ar radio-frequency (rf) discharge in film deposition environment was investigated experimentally using a rf sputtering system without magnetron, and the observed effects of process conditions, such as absorbed rf power, substrate bias voltage, working pressure, and gas flow rate on the rf discharge were interpreted in terms of energy balance and sheath capacitance considerations. It was shown that the Ar gas flow had a marginal effect on the discharge. However, the absorbed rf power, substrate bias voltage, and working pressure exhibited strong effects on the target self-bias voltage and ion current density in the discharge, and the energy delivery from the source to the discharge was efficient when these parameters were set in the optimized range.

I. INTRODUCTION

Sputtering techniques are widely used to deposit thin films of thickness ranging from a few nanometers to hundreds of nanometers. Low-pressure radio-frequency (rf) discharge has been extensively studied both experimentally and theoretically (Koening et al., 1970; Coburn et al., 1972; Keller et al., 1979; Köhler et al., 1985; Köhler et al., 1985; Metze et al., 1986; Lieberman, 1988; Manenschijn et al., 1991; Lieberman et al., 1994; Miller et al., 1997; Panagopoulos et al., 1999), and the dynamics of rf plasma sheaths have attracted significant attention due to their importance in various rf discharge applications. For all radio frequencies, there is a critical parameter, $\omega\tau_i$, that controls the ion modulation in the rf sheath, where ω is the frequency of the applied field, and τ_i is the ion transit time through the sheath. Neglecting the ion entering velocity (Bohm velocity) at the sheath edge and assuming a collisionless sheath, τ_i is given by (Panagopoulos et al., 1999)

$$\tau_i = 3S\sqrt{\frac{m_i}{2eV_{sh}}}, \tag{1}$$

where m_i is the ion mass, S and V_{sh} are the sheath thickness and sheath voltage, respectively, and e is the elementary charge. For low frequencies and/or short ion transit time ($\omega\tau_i << 1$), the variation of ion bombarding energies at both target and substrate surfaces follows the variation of the corresponding sheath voltages because the ions are subjected to the sheath voltages occurring at the time they enter the sheaths. For high frequencies and/or long ion transit time ($\omega\tau_i >> 1$), the ions respond to time-average sheath voltages because they are subjected to various field oscillations during travel through the sheaths. In low-pressure Ar rf discharge (13.56 MHz), the ions respond only to time-average electrical fields because $\omega\tau_i >> 1$. The powers dissipated in the

two electrode sheaths are the entire source of power that maintains the discharge during capacitive excitation, and the plasma bulk usually defines the boundary conditions of the sheath problem. Lieberman (1988) analyzed theoretically the capacitive rf sheath for time-independent, collisionless ion motion in the sheath and inertialess electrons ($\omega\tau_i >> 1$). The unique feature in Lieberman's model is the assumptions that the electron density is equal to the ion density at the sheath edges and zero at the electrodes. Metze et al. (1986) analyzed the sheath voltage waveforms using an equivalent circuit model of a plasma reactor for the transit time τ_i of ions through the sheath less than $1/f$, where f is the frequency of the applied voltage. In this model, the sheath thickness corresponds to the steady-state thickness related to the instantaneous voltage $V_{sh}(t)$ across the sheath. So this model is a quasi-steady-state model and is valid for frequency less than 1 MHz for Ar plasmas of ion density equal to 10^{10} cm^{-3}. Miller et al. (1997) developed a semi-analytical model to connect both extremes.

In this study, A Perkin-Elmer Randex-2400 model sputtering system without magnetron shown schematically in Figure 1 was used to study the characteristics of low-pressure Ar rf discharge. The plasma was excited and maintained by a rf power supply through a rf coupling coil and capacitive tuning network (Figure 2). A bias voltage can be applied to the substrate by the substrate bias tuning technique. In low-pressure Ar rf discharge, the target is negatively self-biased. Relationships including the rf power, substrate bias voltage, and target negative self-bias voltage were obtained for low-pressure Ar rf discharge. An expression for the ion current density was derived from energy balance considerations.

II EXPERIMENTAL PROCEDURES

The geometry configuration of the rf discharge in the Perkin-Elmer Randex-2400 model sputtering system is symmetric, the target surface area A_T is equal to the substrate area A_S, and the substrate is 200 mm in diameter. The spacing between the two electrodes (target and substrate) is fixed at 7 cm. During low-pressure Ar rf discharge, the temperatures of both target and substrate are maintained at room temperature by water cooling, the working pressure is set by adjusting the opening of a throttle valve (Figure 1), the gas flow rates are regulated by MKS flow ratio controllers, and the forward rf power generated by rf power supply is servo-stabilized in the range of 80 - 1000 W. The power that sustains the discharge is called absorbed rf power, which is usually not equal to the forward rf power due to the impedance mismatch between the rf power supply and the plasma. The power difference between them is called the reflected rf power. Both the forward and reflected rf powers are regulated during the low-pressure Ar rf discharge.

For low-pressure rf Ar gas discharge, the vacuum chamber was pumped down to a low base pressure (< 2 x 10^{-6} Torr) by a turbo molecular pump backed by a rotary mechanical pump to reduce the effects of residual air before introducing Ar gas into the chamber (Figure 1). The base pressure was measured by a Granville-Philips ion gauge. During low-pressure Ar rf discharge, the substrate bias and target self-bias voltages were measured directly. The effects of forward rf power, substrate bias voltage, working pressure and Ar gas flow rate on the target self-bias voltage and ion current density were investigated experimentally and representative results were discussed.

III RESULTS AND DISCUSSION

A. Radio-frequency power dependence of ion current density and electrode bias potentials

Electrically, plasma sheaths generated in low-pressure rf discharge can be modeled as pure capacitors when $\omega\tau_i >> 1$, and the sheath behavior can be analyzed using an equivalent electrical circuit of the discharge (Koening et al., 1970; Coburn et al., 1972; Keller et al., 1979; Köhler et al., 1985; Köhler et al., 1985; Manenschijn et al., 1991; Lieberman et al., 1994). For a parallel-plate capacitor, the capacitance C

$$C = \frac{\varepsilon_o \varepsilon_d A}{S}, \tag{2}$$

where ε_o is the electrical permittivity in vacuum (= 8.8542 x 10^{-12} F/m), ε_d is the dielectric constant of the capacitor medium, A is the plate area ($A = A_T = A_S = 324\,\text{cm}^2$ in the present sputtering system). For low-pressure rf discharge, ε_d is determined by the working gas, working pressure, and electrical power, whereas the areas of the two electrodes are fixed. The capacitance varies with time due to the oscillation of the sheath thickness $S(t)$. This oscillation produces a displacement current (displacement of electrons) which represents the reflected rf power P_r. The reflected power can overload the power supply, and thus preventing effective delivery of the power to the discharge in the absence of an impedance matching network between the power source and the plasma. Figure 2 shows a schematic of the electrical power matching network used in the present sputtering system. A single power supply is used, and the rf power is split between the target and the substrate electrodes. Figure 3 shows the equivalent electrical circuit (Koening et al., 1970).

Assuming that the ion density n_i is equal to the electron density n_e in the bulk of the plasma and that the electrons are in thermal equilibrium with the local plasma potential (Boltzmann-Maxwellian distribution), the ion current density j through the sheath can be expressed as (Smith, 1995)

$$j = 0.6 n_e e \sqrt{\frac{k_B T_e}{m_i}}, \tag{3}$$

where T_e is the electron temperature (degree in Kelvin) of a Boltzmann-Maxwellian distribution, k_B is the Boltzmann constant. The ion current densities in both sheaths are determined by the electron temperature and density in the plasma bulk. T_e is determined by particle conservation alone, and is independent of n_e and, therefore, input power. T_e is weakly dependent on the working pressure. n_e is determined by the total power balance in the discharge and is a function of pressure. It can be expressed as (Lieberman et al., 1994)

$$n_e = \frac{P_a}{e u_B A_{eff} \varepsilon_T}, \tag{4}$$

where P_a and $u_B = \sqrt{\frac{eT_e}{m_i}}$ are the absorbed rf power and Bohm velocity, respectively, ε_T is the total energy lost per ion lost from the system, and A_{eff} is the effective area given by (Lieberman et al., 1994)

$$A_{eff} = A(h_l + \frac{l}{R} h_{R)}, \tag{5}$$

where $l \approx 7\,\text{cm}$ and $R = 100\,\text{mm}$ are the discharge length and electrode radius, respectively, and $h_l \approx 0.86(3 + \frac{l}{2\lambda_i})^{-1/2}$ and $h_R \approx 0.80(4 + \frac{R}{\lambda_i})^{-1/2}$ represent the effects of working pressures on the ion distributions at the axial and radial sheath edges, where λ_i is the mean free path of ions. The total energy lost per ion lost from the system ε_T is given by (Lieberman et al., 1994)

$$\varepsilon_T = \varepsilon_C + 2T_e + \varepsilon_i, \tag{6}$$

where ε_C, $2T_e$, and ε_i represent the energy loss per electron-ion pair created, the mean kinetic

energy lost per electron lost from the system, and the mean kinetic energy lost per ion across the sheath.

Hence, the ion current density j through the sheath is determined by the absorbed power P_a and electron temperature T_e, and can be expressed as

$$j = j_T = j_S = \frac{P_a}{\varepsilon_T} f(T_e), \tag{7}$$

where j_T and j_S are ion current densities into the target and substrate sheaths, respectively. The ion current density j is linearly dependent on $\frac{P_a}{\varepsilon_T}$ for $T_e \approx$ constant.

For monatomic gas (e.g., Ar) discharge at low pressure and high power, all the absorbed power P_a is responsible for ion acceleration across the sheaths (Godyak et al., 1991). For a symmetric rf discharge geometry, the absorbed power P_a is given by

$$P_a = j(\Delta V_T + \Delta V_S)A, \tag{8}$$

where $\Delta V_T = V_p - V_T$ and $\Delta V_S = V_p - V_S$ are voltage differences across the target and substrate sheaths, respectively, where V_p is the time-average plasma bulk voltage (≈ 10 V), and V_T and V_S are the time-average voltages at the target and substrate surfaces, respectively. From Eq. (8), the ion current density j can be obtained from the measured P_a, V_T, V_S, i.e.,

$$j = \frac{P_a}{A(2V_P - V_T - V_S)}, \tag{9}$$

where electrode area A (= 324 cm^2) is given for present sputtering system. Figure 4 shows the variation of the ion current density j with the absorbed rf power P_a for low-pressure Ar rf discharge under conditions of substrate bias voltage of –200 V, working pressure of 3 mTorr, and

Ar gas flow rate of 20 sccm. The ion current density increased with absorbed rf power, agreeing well with the prediction of Eq. (7).

The time-average voltage across the sheath is given by (Lieberman et al., 1994)

$$\overline{V} \propto \frac{j^2}{e\varepsilon_o n_e \omega}. \tag{10}$$

Therefore, the time-average voltages across the target sheath can be expressed as

$$V_T = -\frac{P_a}{Aj} + 2V_P - V_S \propto \frac{u_B A_{eff}}{\varepsilon_o \omega} f^2(T_e)\frac{P_a}{\varepsilon_T}. \tag{11}$$

From Eq. (11), it is obvious that the target is negatively self-biased because $\frac{P_a}{Aj} >> 2V_P - V_S$. For high sheath potential, $\varepsilon_T \approx \varepsilon_i$ because $\varepsilon_i >> \varepsilon_C$ and $\varepsilon_i >> T_e$. Roughly, $\varepsilon_i \approx e|V_T|$. Therefore,

$$V_T \propto \left(\frac{u_B A_{eff}}{\varepsilon_o \omega e}\right)^{1/2} f(T_e) P_a^{1/2}. \tag{12}$$

The absolute value of the target self-bias voltage V_T increases with the square root of the absorbed rf power P_a for fixed substrate bias voltage V_S. Figure 4 also shows the variation of target self-bias voltage V_T with absorbed rf power P_a. The experimental results agree well with the prediction of Eq. (12).

Eq. (11) shows that $V_T + V_S$ is constant when the absorbed rf power P_a is fixed. Hence, the absolute value of V_T will decrease with increasing absolute value of negative V_S. Figure 5 shows the variation of V_T and $V_T + V_S$ with V_S for low-pressure Ar rf discharge under conditions of forward rf power P_f of 750 W, working pressure of 3 mTorr, and gas flow rate of 20 sccm. The results show that the experimental trends are in good agreement with the above interpretations for substrate bias voltages between 0 and –300 V. As shown in Figure 5, $V_T + V_S$ decreased with the

decrease of V_S below –300 V. This is because the absorbed rf power P_a decreased when the negative substrate bias voltage was less than -300 V, as shown in Figure 6. The substrate was not self-biased. The negative substrate bias voltage V_S was applied independently through the substrate bias adjuster (Figure 2). The change in V_S affected the impedance Z_S between the substrate and the bulk of plasma and the impedance Z_{SG} between the substrate and the ground (Figure 3), resulting in the change of the total impedance of the plasma, which produced a mismatch between the impedances of the rf source and the plasma. The mismatch impedances prevented the rf source from delivering efficiently power to the plasma, resulting in the decrease of the absorbed rf power P_a even though the forward rf power P_f was fixed at 750 W. Therefore, the system must be tuned to match the impedances of the rf source and the plasma. The present system was tuned to work well for substrate bias voltage in the range of 0 to -300 V. In this range, the reflected rf power P_r is less than 3% of the forward rf power P_f.

The variation of the forward rf power P_f may cause changes in the rf source impendence, which can also lead to a mismatch between the impedances of the rf source and the plasma and prevent the rf source from efficiently delivering power to the plasma. Figure 7 shows the effect of the forward rf power P_f on the absorbed rf power P_a for Ar rf discharge under conditions of substrate bias voltage V_S of -200 V, working pressure of 3 mTorr, and gas flow rate of 20 sccm. The ratio of P_a / P_b increased with the forward rf power P_f. For forward rf power P_f between 400 to 750 W, the absorbed rf power P_a was larger than 95% forward rf power P_f. However, when the forward rf power P_f was less than 400 W, the ratio of P_a / P_b decreased dramatically with the decrease of the forward rf power P_f.

B. Effects of working pressure and gas flow rate on low-pressure rf discharge

The significance of working pressure and gas flow rate on low-pressure Ar rf discharge was investigated experimentally under conditions of forward rf power P_f of 750 W and substrate bias voltage V_S of -200 V. The working pressure can be adjusted by controlling the throat valve opening (Figure 1). However, the adjustable range of the working pressure is limited by the Ar gas flow rate. Figure 8 shows the Ar gas flow rate dependence of the adjustable range of the working pressure. The adjustable range of working pressure increased with the Ar gas flow rate. Figures 9 - 11 show the variations of absorbed rf power P_a, ion current density j, and target self-bias voltage V_T, respectively, with the working pressure and Ar gas flow rate. The results show that the gas flow rate had secondary effect on the low-pressure Ar rf discharge. However, the working pressure had a significant effect on this discharge. The absorbed rf power P_a increased with increasing working pressure continuously, reaching a maximum at ~2.5 mTorr, and then decreased above ~2.5 mTorr working pressure (Figure 9). Alternatively, the ion current density j increased and the target self-bias voltage V_T decreased with increasing working pressure, both reaching steady-state values for the working pressure greater than 2.5 mTorr (Figures 10 and 11).

At low pressures (<10 mTorr), the pressure effect on the sheath thickness is marginal (Pennebake, 1979). As mentioned previously, the electron temperature T_e is weakly dependent on the working pressure. However, increasing the pressure enhances both the discharge rate of Ar atoms and the recombination rate between electrons and ions due to the increase of particle collisions in the bulk plasma space. The mean free path of particles in the bulk plasma space is given by

$$\lambda = \frac{k_B T}{\sqrt{2}\pi d^2 p}, \tag{13}$$

where T , d , and p are the temperature of the bulk plasma, particle diameter and working pressure, respectively. Eq. (13) shows that the electron mean free path is significantly longer than that of the Ar ions due to the smaller size of the electrons. Hence, the increase of the recombination rate between electrons and Ar ions is less than the discharge rate of Ar atoms. This leads to an increase in the Ar ion density n_i in the bulk plasma with an increase in the working pressure, which equals the electron density n_e. In view of Eq. (3), the ion current density j increases with n_e. The experimental trend shown in Figure 10 is in good agreement with the former interpretation. The increase of the Ar ion density in the bulk plasma changed the plasma impedance, thus, producing a mismatch between the rf source and plasma impedances, which leaded to the decrease of the absorbed rf power P_a. This is the reason why the absorbed rf power P_a decreased for the working pressure above 2.5 mTorr (Figure 9). The decrease of the absorbed rf power P_a leaded to a decrease in the target self-bias voltage V_T , as indicated by Eq. (12).

IV CONCLUSIONS

Relationships including the forward rf power, substrate bias voltage, and target self-bias voltage were observed in experiments at different conditions of low-pressure Ar rf discharge performed in a Perkin-Elmer sputtering system without magnetron. The effects of the forward rf power, substrate bias voltage, working pressure, and Ar gas flow rate on the target self-bias voltage and ion current density were interpreted in the context of both energy balance and sheath capacitance considerations. It is found that the Ar gas flow rate only determined the adjustable range of the working pressure, while its effect on the discharge was secondary. However, the

forward rf power, substrate bias voltage, and working pressure exhibited strong effects on the plasma discharge, and the energy delivery from the rf source to the discharge was most efficient when the former parameters were in their optimized ranges.

ACKNOWLEDGEMENTS

This research was supported by the National Science Foundation (Grant No. CMS-9734907) and the Computer Mechanics Laboratory at the University of California at Berkeley.

REFERENCES

Koening, H. R. and Maissel, L. I., Application of r.f. discharges to sputtering, *IBM J. Res.Develop.* ***14***, 168 (1970).

Coburn, J. W. and Kay, E., Positive-ion bombardment of substrate in rf diode glow discharge sputtering, *J. Appl. Phys.* ***43***, 4965 (1972).

Keller, J. H. and Pennebake, W. B., Electrical properties of RF sputtering systems, *IBM J. Res. Develop.* ***23***, 3 (1979).

Köhler, K, Coburn, J. W., Horne, D. E., Kay, E. and Keller, J. H., Plasma potentials of 13.56-MHz argon glow discharges in a planar system, *J. Appl. Phys.* ***57***, 59 (1985).

Köhler, K., Horne, D. E. and Coburn, J, W., Frequency dependence of ion bombardment of grounded surfaces in rf argon glow discharges in a planar system, *J. Appl. Phys.* ***58***, 3350 (1985).

Metze, A., Ernie, D. W. and Oskam, H. J., Application of the physics of plasma sheaths to the modeling of rf plasma reactors, *J. Appl. Phys.* ***60***, 3081 (1986).

Lieberman, M. A., Analytical solution for capacitive RF sheath, *IEEE Trans. Plasma Sci.* ***16***, 638 (1988).

Manenschijn, A., Janssen, G. C. A. M., van der Drift, E. and Radelaar, S., Measurement of ion impact energy and ion flux at the rf electrode of a parallel plate reactive ion etcher, *J. Appl. Phys.* ***69***, 1253 (1991).

Lieberman, M. A. and Lichtenberg, A. J., *Principles of Plasma Discharges and Materials Processing* (John Wiley & Sons, Inc., New York, 1994).

Miller, P. A. and Riley, M. E., Dynamics of collisionless rf plasma sheaths, *J. Appl. Phys.* ***82***, 3689 (1997).

Panagopoulos, T. and Economou, D. J., Plasma sheath model and ion energy distribution for all radio frequency, *J. Appl. Phys.* ***85***, 3435 (1999).

Smith, D. L., *Thin-Film Deposition: Principles and Practice* (McGraw-Hill, New York, 1995), Ch. 8 & 9.

Godyak, V. A., Piejak, R. B. and Alexandrovich, B. M., Ion flux and ion power losses at the electrode sheaths in a symmetrical rf discharge, *J. Appl. Phys.* ***69***, 3455 (1991).

Pennebake, W. B., Influence of scattering and ionization on RF impedance of glow discharge sheaths, *IBM J. Res. Develop.* ***23***, 16 (1979).

LIST OF FIGURES

Figure 7 The effect of forward rf power P_f on the level of absorbed rf power P_a for low-pressure Ar rf discharge under conditions of substrate bias voltage V_S of -200 V, working pressure of 3 mTorr and gas flow rate of 20 sccm.

Figure 8 Ar gas flow rate dependence of working pressure adjustable range.

Figure 9 Effects of working pressure and gas flow rate on the absorbed rf power P_a for low-pressure Ar rf discharge under conditions of forward rf power P_f of 750 W, and substrate bias voltage V_S of –200 V.

Figure 10 Effects of working pressure and gas flow rate on ion current density j for low-pressure Ar rf discharge under conditions of forward rf power P_f of 750 W, and substrate bias voltage V_S of –200 V.

Figure 11 Effects of working pressure and gas flow rate on target self-bias voltage V_T for low-pressure Ar rf discharge under conditions of forward rf power P_f of 750 W, and substrate bias voltage V_S of –200 V.

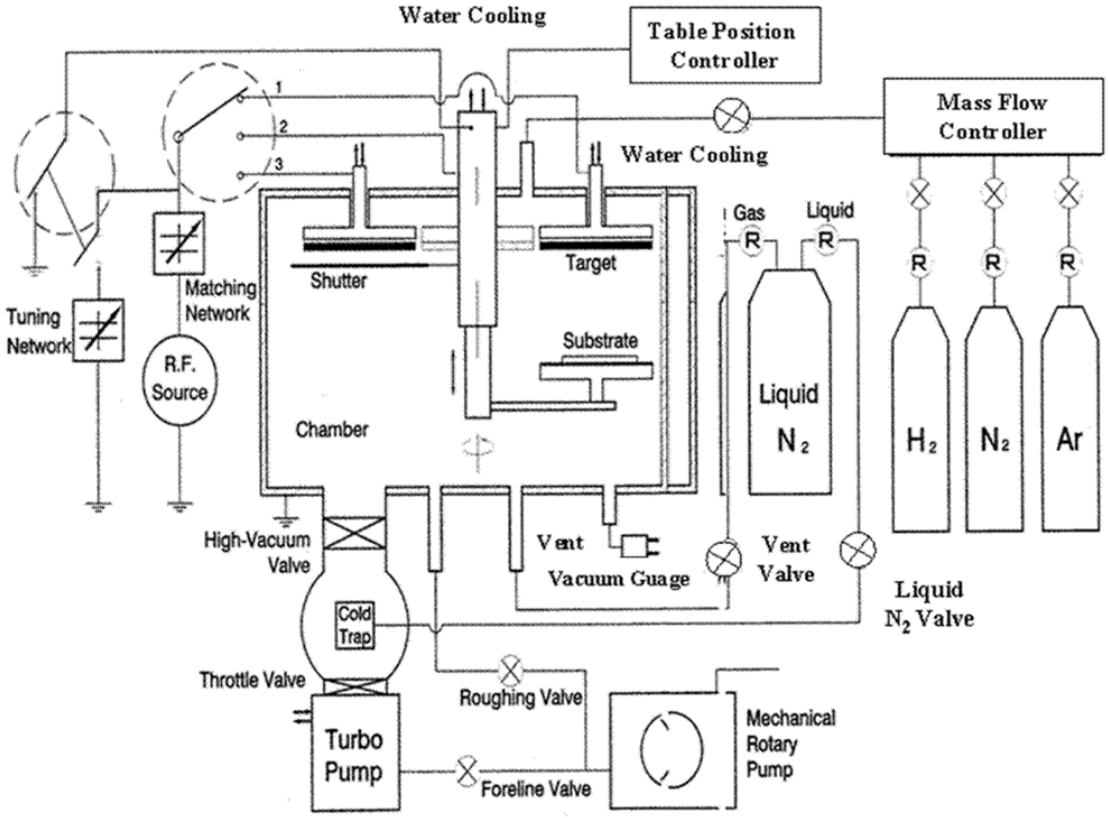
Water Cooling
Table Position Controller
Mass Flow Controller
Water Cooling
1
2
3
Gas
Liquid
R
Shutter
Target
Substrate
Matching Network
Tuning Network
R.F. Source
Chamber
Liquid N_2
H_2
N_2
Ar
High-Vacuum Valve
Vent
Vacuum Guage
Vent Valve
Liquid N_2 Valve
Cold Trap
Throttle Valve
Roughing Valve
Turbo Pump
Foreline Valve
Mechanical Rotary Pump

Figure 1

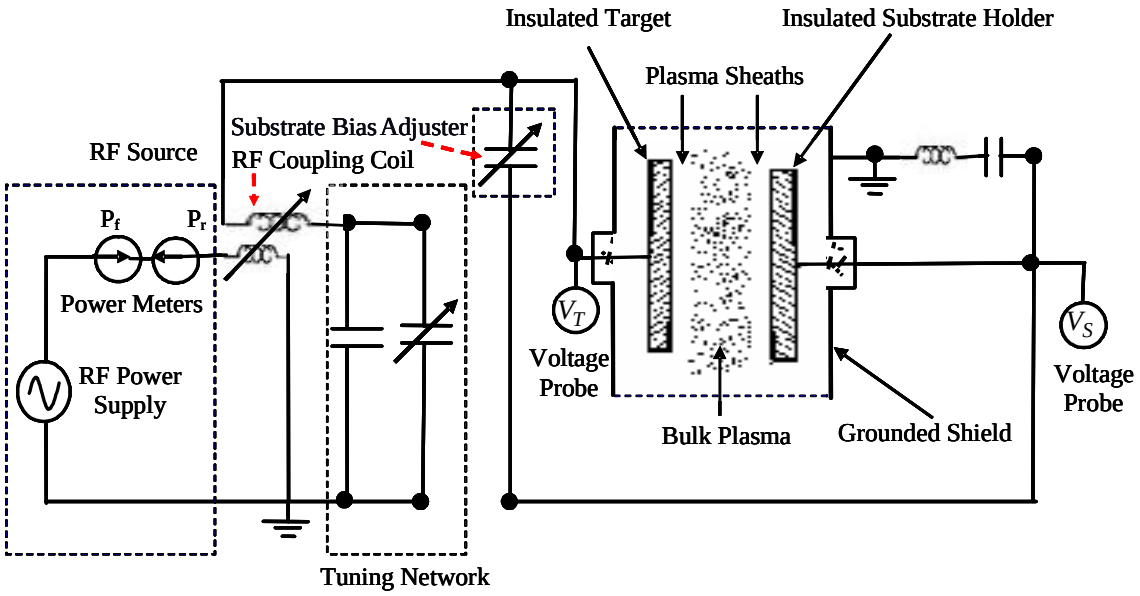
Insulated Target
Insulated Substrate Holder
Plasma Sheaths
Substrate Bias Adjuster
RF Coupling Coil
RF Source
P_f
P_r
Power Meters
RF Power Supply
V_T
Voltage Probe
V_S
Voltage Probe
Bulk Plasma
Grounded Shield
Tuning Network

Figure 2

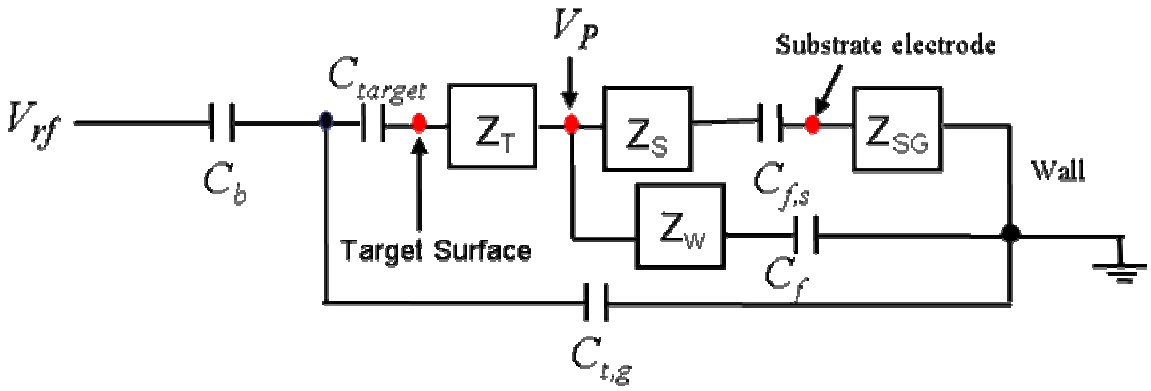
V_{rf}
C_b
C_{target}
Target Surface
Z_T
V_P
Z_S
Substrate electrode
Z_{SG}
$C_{f,s}$
Wall
Z_W
C_f
$C_{t,g}$

Figure 3

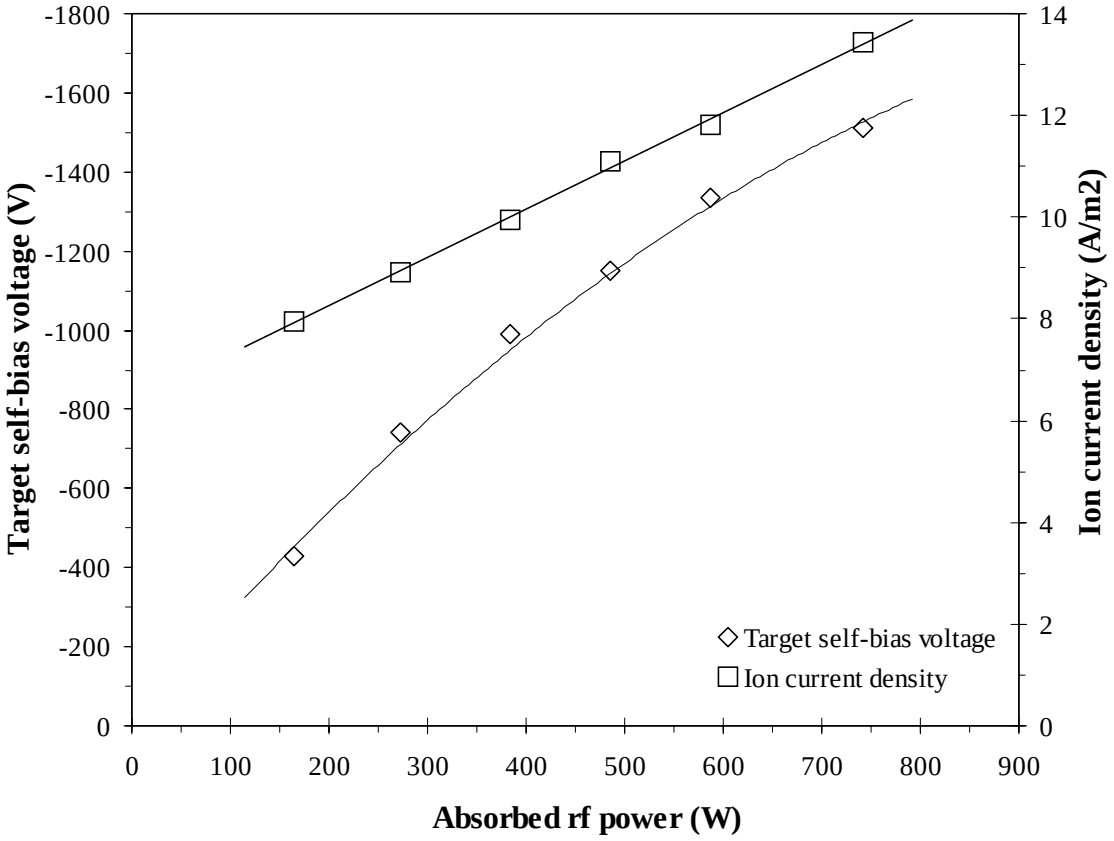
-1800
-1600
-1400
-1200
-1000
-800
-600
-400
-200
0
Target self-bias voltage (V)
14
12
10
8
6
4
2
0
Ion current density (A/m2)
0
100
200
300
400
500
600
700
800
900
Absorbed rf power (W)
Target self-bias voltage
Ion current density

Figure 4

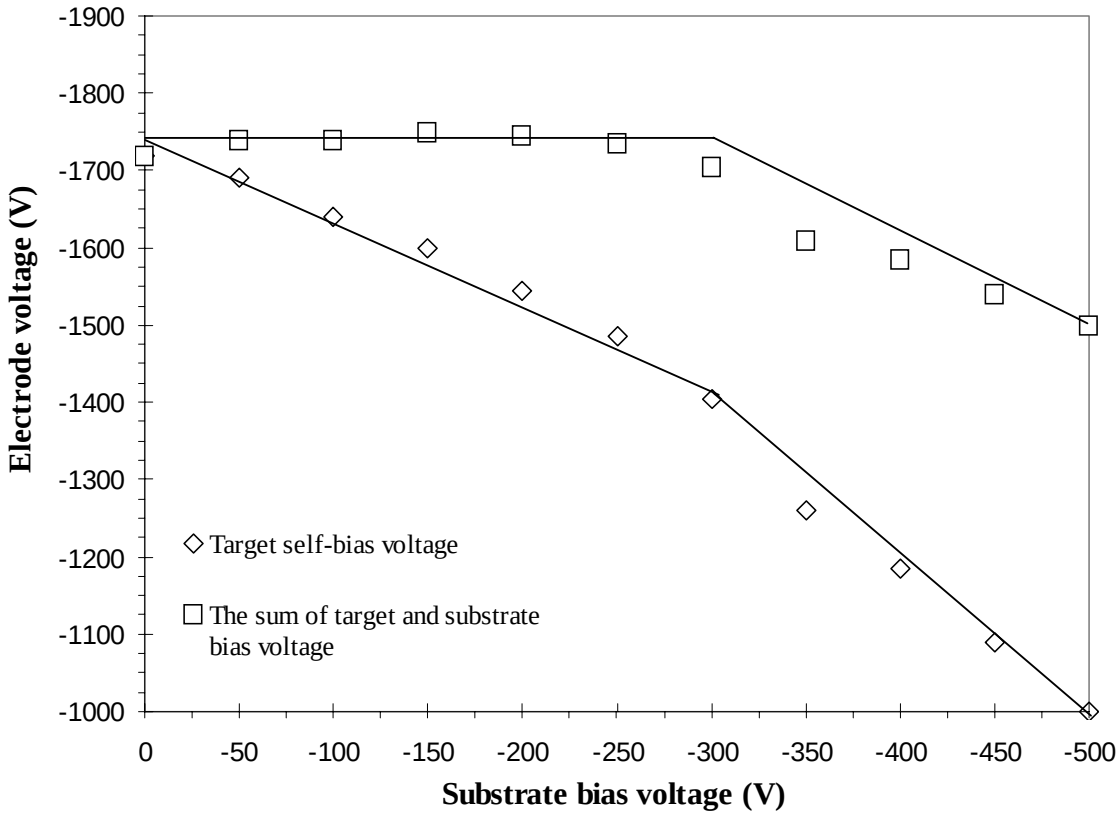
-1900
-1800
-1700
-1600
-1500
-1400
-1300
-1200
-1100
-1000
Electrode voltage (V)
0
-50
-100
-150
-200
-250
-300
-350
-400
-450
-500
Substrate bias voltage (V)
Target self-bias voltage
The sum of target and substrate bias voltage

Figure 5

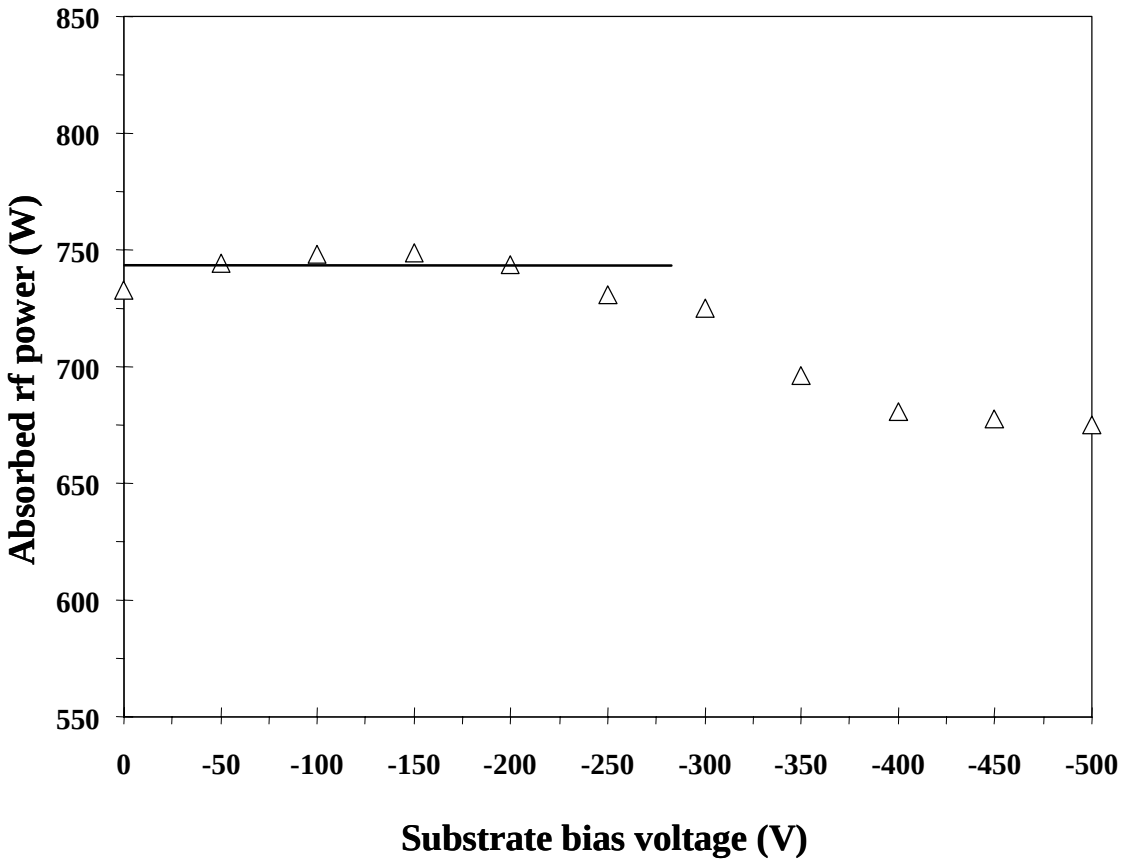
850
800
750
700
650
600
550
Absorbed rf power (W)
0
-50
-100
-150
-200
-250
-300
-350
-400
-450
-500
Substrate bias voltage (V)

Figure 6

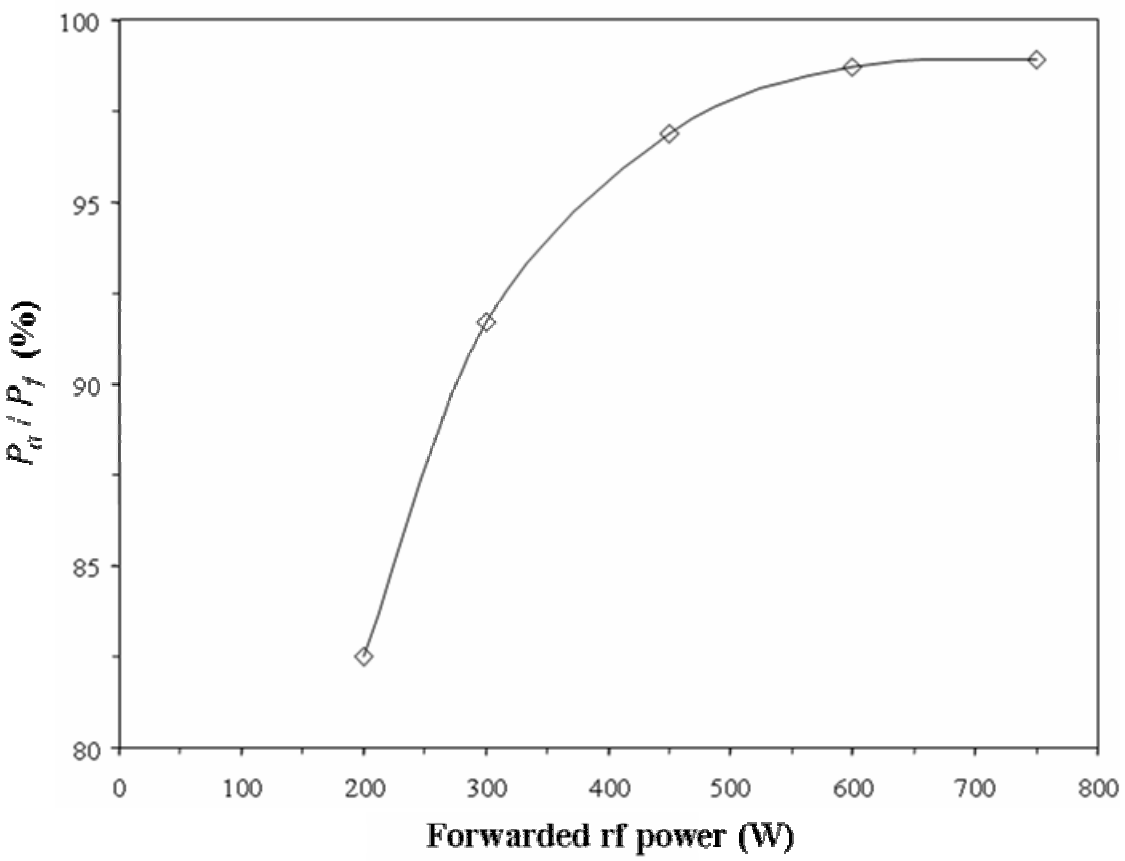
100
95
90
85
80
0
100
200
300
400
500
600
700
800
P_R / P_f (%)
Forwarded rf power (W)

Figure 7

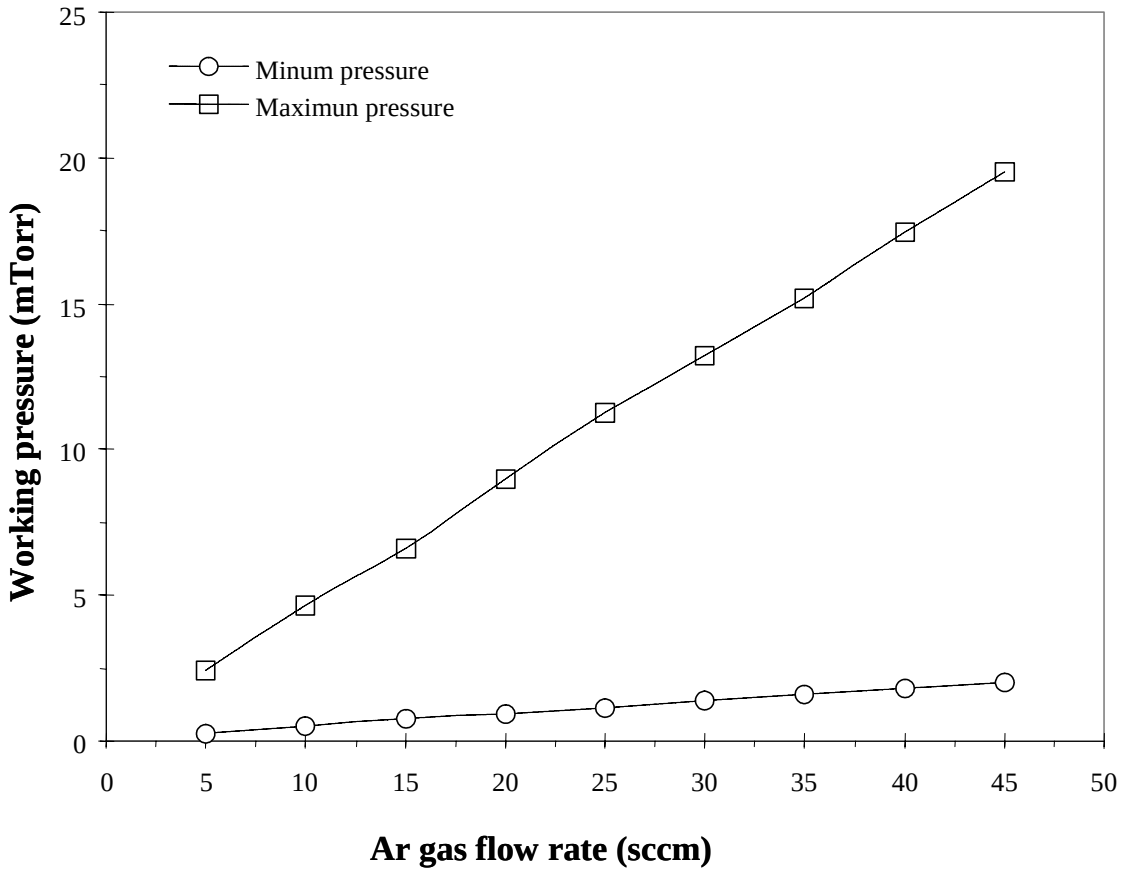
Minum pressure
Maximun pressure
Working pressure (mTorr)
Ar gas flow rate (sccm)
0
5
10
15
20
25
30
35
40
45
50

Figure 8

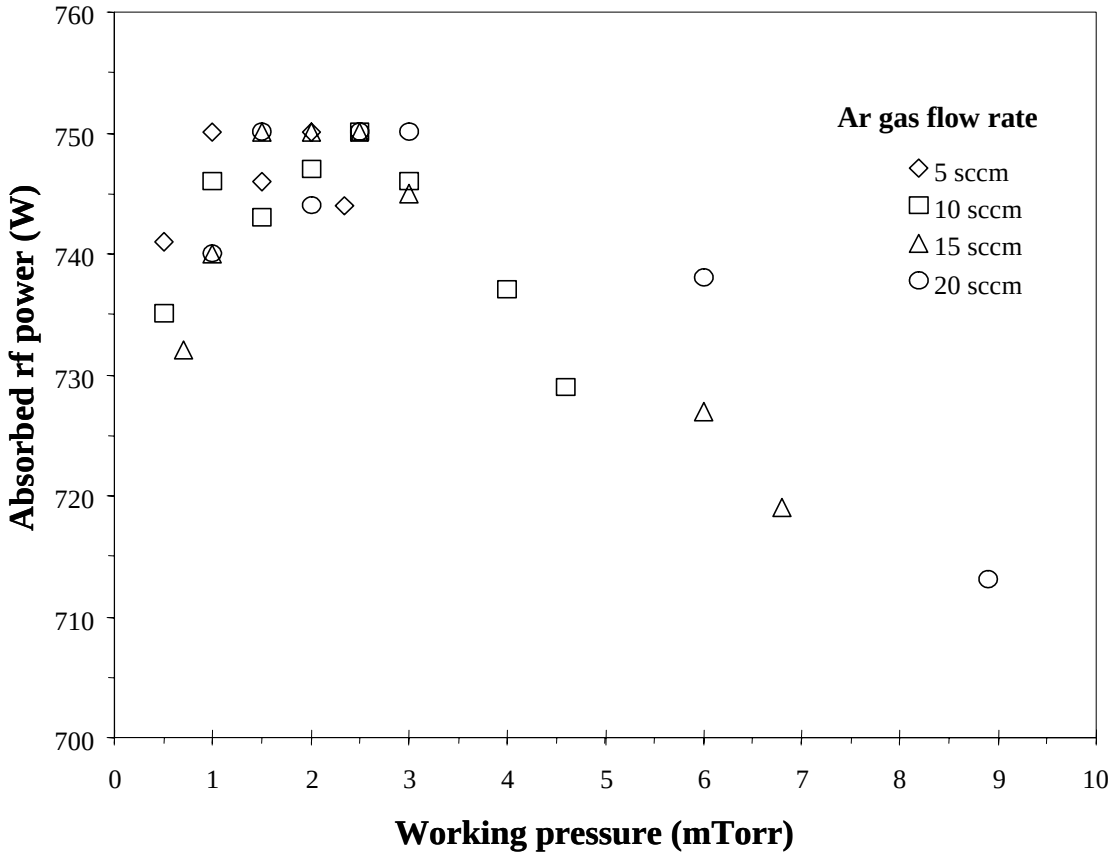
760
750
740
730
720
710
700
0
1
2
3
4
5
6
7
8
9
10
Absorbed rf power (W)
Working pressure (mTorr)
Ar gas flow rate
5 sccm
10 sccm
15 sccm
20 sccm

Figure 9

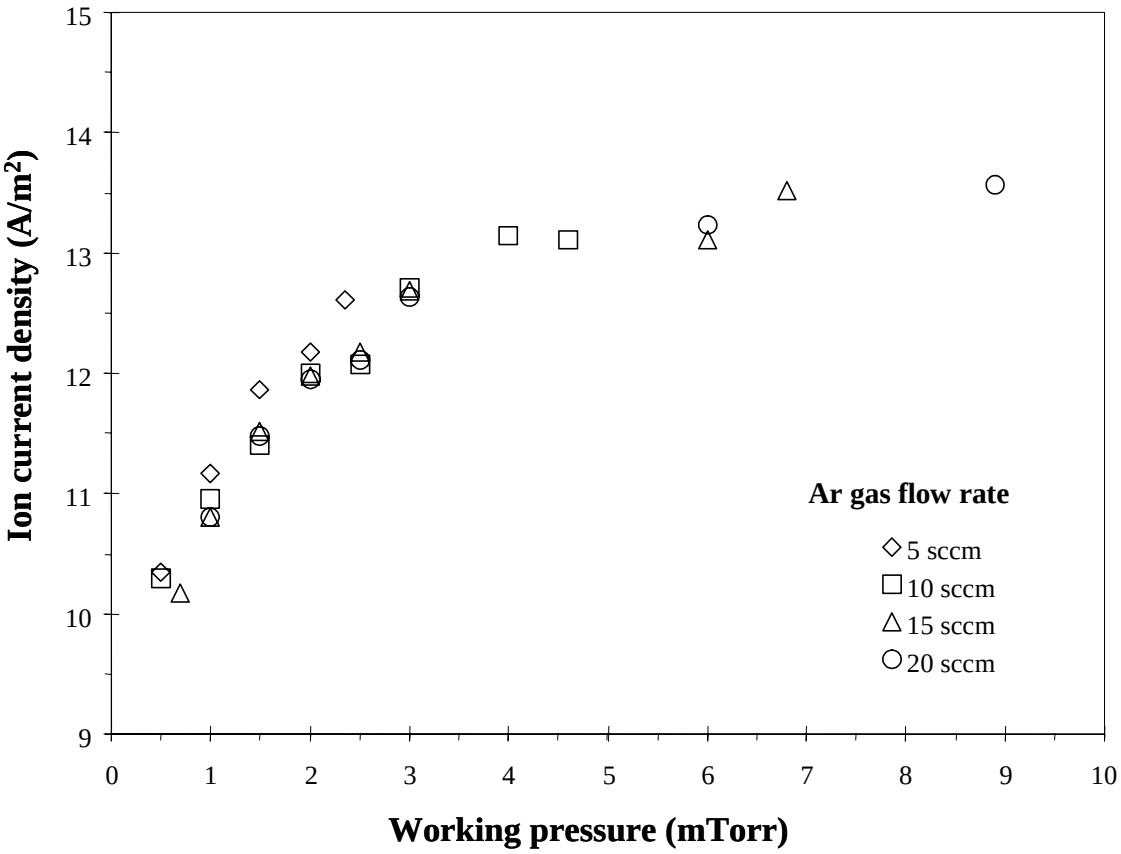
Ion current density (A/m²)
Working pressure (mTorr)
Ar gas flow rate
5 sccm
10 sccm
15 sccm
20 sccm
15
14
13
12
11
10
9
0
1
2
3
4
5
6
7
8
9
10

Figure 10

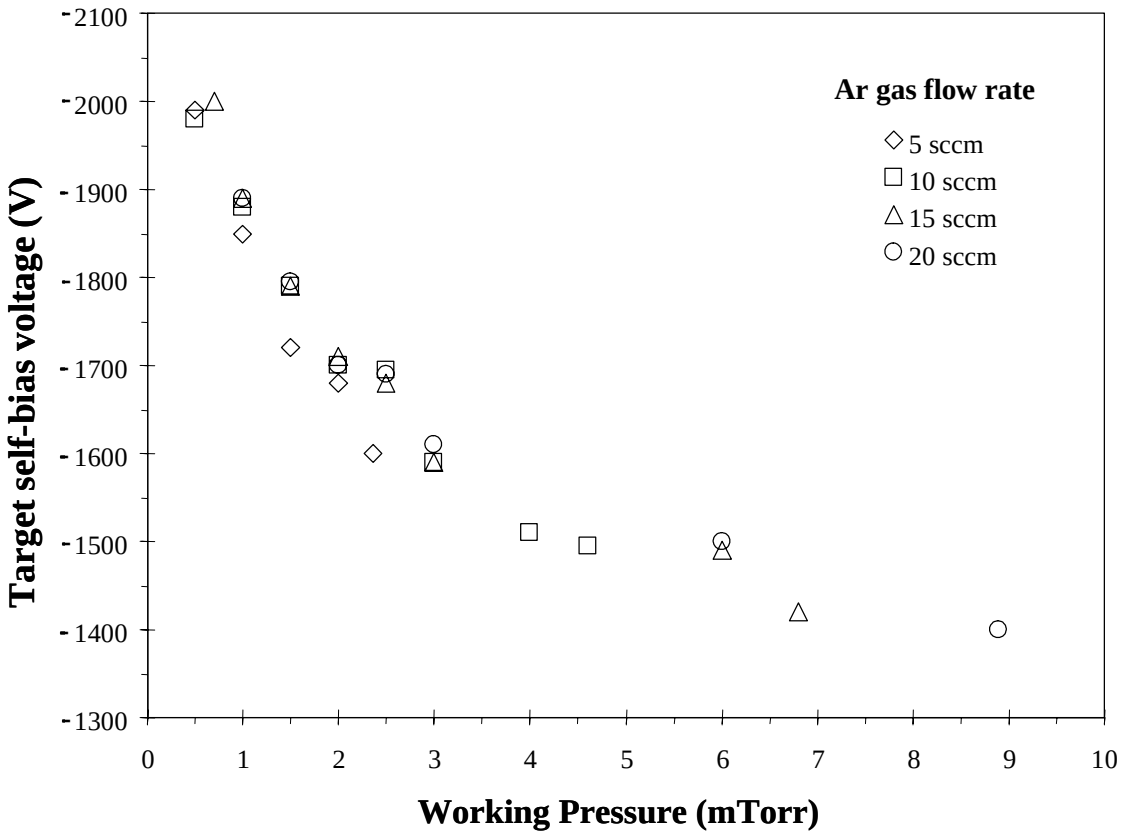
Target self-bias voltage (V)
2100
2000
1900
1800
1700
1600
1500
1400
1300
0
1
2
3
4
5
6
7
8
9
10
Working Pressure (mTorr)
Ar gas flow rate
5 sccm
10 sccm
15 sccm
20 sccm

Figure 11